A NOVEL APPROACH TO MODELING EMISSIVITY AND ALBEDO OF THE MARTIAN SEASONAL CAPS. J. Eluszkiewicz[1] and T. N. Titus[2], [1]Atmospheric and Environmental Research, Inc., 131 Hartwell Ave., Lexington, MA 02421, jel@aer.com, [2]U.S. Geological Survey, 2255 North Gemini Dr., Flagstaff, AZ 86001, ttitus@usgs.gov.

Summary: Initial results from a new model for the emissivity and reflectivity of the martian seasonal caps represented as porous slabs are described. The radiative transfer modeling is linked to a physically based model of CO_2 frost metamorphism. Besides Mars, this coupled radiative transfer/sintering model is applicable to other Solar System bodies where slab-like volatile deposits are likely to be present, including Triton, Pluto, and Io.

Introduction: There is abundant evidence that large portions of the seasonal CO_2 deposits in the polar regions of Mars form a solid slab rather than a fluffy frost. The presence of low-porosity slabs of solid CO_2 was indicated by the early spectroscopic measurements of the caps that suggested long (on the order of 10 cm) path lengths in the 1.5-μm absorption band of solid CO_2 [1,2]. Unusually long spectroscopic path lengths for portions of the seasonal caps were subsequently inferred from later observations [3,4]. Viking images [5] revealed that the southern residual cap could be distinguished when the seasonal frost was present and that it was always brighter than the brightest areas in the seasonal cap, thus strongly arguing for some degree of transparency in the seasonal deposits. With partially transparent seasonal caps, the albedo contrast between the northern and southern residual caps, invoked to explain the compositional dichotomy between the residual caps (H_2O in the north, CO_2 in the south) [6] could reside in the residual caps. This would make the albedo contrast permanent, whereas in the alternative hypothesis of dust contamination of the overlying seasonal deposits the contrast would be sporadic (e.g., related to the occurrence of dust storms). Furthermore, the penetration of sunlight through a clear CO_2 layer would help to stabilize the compositional dichotomy [7].

The above observations and modeling results led to the conclusion that a semitransparent seasonal CO_2 slab forms on Mars by pressureless sintering [8]. According to this model, the slab is polycrystalline and the long path lengths result from the elimination of voids between crystals. This densification process is driven by the thermodynamic requirement of minimum surface energy and its kinetics is determined by the material properties of solid CO_2, crystal size, and temperature. In addition, circumstances specific to Mars, e.g., the near-absence of an inert gas, low abundance of impurities, and nearly isothermal conditions, are conducive to the formation of low-density CO_2 deposits. These factors distinguish the CO_2 frost metamorphism on Mars from the snow metamorphism of Earth. On the other hand, CO_2 metamorphism on Mars has many analogs to the N_2 frost metamorphism on Triton [9], where the preponderance of evidence also points out to the presence of semi-transparent seasonal deposits [10-14]. Interestingly, a spectacular phenomenon observed on Triton, the presence of active geysers and dark streaks apparently caused by geyser-like eruptions [15], may have a counterpart on Mars [16]. In both cases, a plausible explanation for these features is offered by a solid-state greenhouse effect occurring in a slab of clear ice [11].

Since 1993, the presence of transparent slabs of solid CO_2 and other results from the sintering model have been supported and/or invoked by numerous studies [17-22]. Most recently, the idea of slab-like CO_2 deposits has been supported by data obtained by instruments onboard the Mars Global Surveyor (MGS) spacecraft. In particular, a densified mean state of the seasonal CO_2 deposits has been inferred from the MOLA and MGS orbital data [23], while very large (up to 1 meter) spectroscopic grain sizes were inferred from analysis of spectra obtained by the Thermal Emission Spectrometer (TES) onboard the spacecraft [24,25]. Slab ice can be distinguished from a porous layer by the shape of the 25-μm band in the TES spectra, with small band depth BD_{25} indicative of small porosity. BD_{25} is defined as the fractional drop in the measured band radiance relative to the expected blackbody radiance at the brightness temperature of adjacent continua [24]. Two sample TES spectra of the southern seasonal cap with small and large BD_{25} are shown in Figure 1. The interpretation of low values of BD_{25} as indicative of slab-like texture has strong physical basis, with zero BD_{25} corresponding to Fresnel reflection [24]. High BD_{25}'s (i.e., low spectral emissivity) have been identified with small grain sizes [24]. In this work, we will instead relate high BD_{25} to high porosity, an interpretation supported both by experimental data on the emissivity of other materials in various stages of densification [26,27] and by new theoretical calculations presented below.

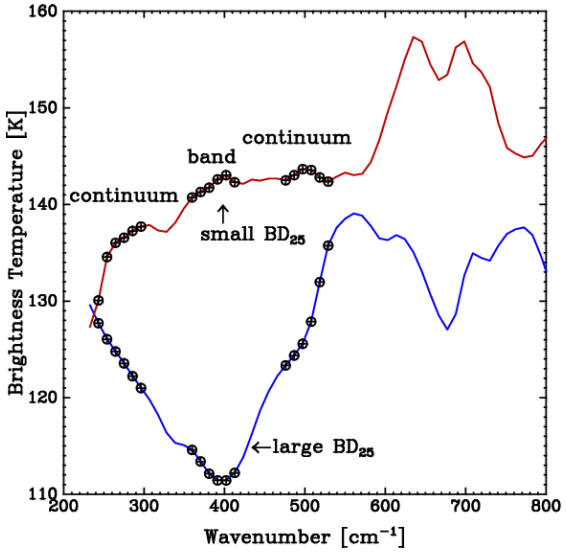

Figure 1: Examples of TES spectra of the southern polar cap. Circles mark spectral locations of channels used to define the 25-μm band (the band itself and two continua). The blue spectrum has low brightness temperatures in the 25-μm band and corresponds to a highly porous deposit. The red spectrum, with a small BD_{25}, corresponds to slab ice.

Texture of Martian Seasonal Caps: The original investigation of the martian CO_2 frost metamorphism [8] only considered densification and led to the conclusion that a slab-like deposit may form on a seasonal timescale provided the frost is sufficiently fine-grained. The TES observations of a CO_2 slab forming essentially simultaneously with deposition in some locations [24], prompted an evaluation of the role played by non-densifying mechanisms in the metamorphism of porous dry ice. The main conclusion from this recent work (and a basic premise of the present study) is that the seasonal CO_2 deposits on Mars rapidly metamorphose into an impermeable slab regardless of the initial grain size. This occurs by the sealing off of the pore space by vapor transport (Kelvin effect). In addition to the TES observations, rapid formation of an impermeable slab is consistent with observations of rapid annealing of microcracks in laboratory samples of dry ice [28,29]. In the laboratory, such rapid annealing leading to the formation of optically clear samples is undoubtedly aided by the favorable geometry of the cracks (crack length >> crack width). In an assembly of spherical grains, the formation of clear samples is likely to be somewhat slower, but a rapid sealing off of the pore space can be rationalized by a consideration of the timescale for sintering due to the Kelvin effect [30]. This mechanism is driven by the difference in curvatures between the neck and the grain surface and stops when this difference becomes zero. In an assemblage of spherical grains, this leads to the formation of isolated spherical pores, which happens when $x \approx 0.3a$, where x and a are the neck and grain diameter, respectively [30]. When the rate equation for neck growth [30] is integrated with the material parameters for solid CO_2 at 142 K (including a recent estimate of surface energy [31]), the timescale to reach this condition is on the order of seconds for a = 1 μm and minutes for a = 10 μm. Even grains as large as 100 μm are likely to develop sealed-off quasi-spherical pores in a matter of hours. It should be emphasized that the Kelvin effect is a non-densifying sintering mechanism that operates in addition to the densifying mechanisms driven by volume and grain-boundary diffusion. Consequently, the slab forming by this mechanism is expected to contain quasi-spherical voids that then undergo slow elimination by the densifying mechanisms. This proposed texture for the martian CO_2 deposits is consistent with the TES and other observations discussed above (in particular, the porous texture of the slab is consistent with the mean density of the seasonal deposits inferred from the MOLA data being less than the theoretical density of solid CO_2) and it has two important consequences for the modeling of the physical properties of the martian seasonal frost. Firstly, the radiative properties of the frost (e.g., albedo and emissivity) are more properly modeled by treating radiative transfer in a slab of solid CO_2 containing spherical voids (and other impurities such as dust grains) rather than by the usual model of spherical CO_2 and dust grains *in vacuo*. In the present study, this problem is tackled by employing the Mie solution for a spherical particle embedded in an absorbing host medium in a multiple scattering code. A second consequence of the impermeability of the slab is the formation of a thermal gradient, which will affect radiative properties of the slab.

Optical Properties of Spherical Particles Embedded in an Absorbing Host Medium: As noted by several authors [32 and references therein], the optical properties of a spherical particle embedded in an absorbing host medium cannot be computed by modifying the refractive indices for the particle and the medium along with scaling the incident wavelength in the input list of the conventional Mie code. Consequently, Yang et al. [32] have considered the general problem when the refractive indices for the particle and the medium have arbitrary values and we rely on their code in the present study. The generalized Mie code can handle both voids and dust particles without difficulty, although a scientific debate continues about the appropriateness of using intrinsic or apparent single scattering properties in multiple scattering calculations [32].

Radiative Transfer in a CO_2 Slab Containing Spherical Voids and Dust Particles: The Mie solution for a spherical particle embedded in an absorbing medium can be applied in a multiple scattering code to compute the radiative properties of the martian CO_2 deposits. In this work, the publicly available DISORT model [33] is used for this purpose. As an example, in Figure 2 we show computed brightness temperatures for an isothermal slab of solid CO_2 at T = 142 K containing spherical voids with 1-μm radius (the refractive indices for solid CO_2 are as in [29]). The choice of this rather small value of r is motivated by the analysis of TES data (see below). As can be seen in Figure 2, the spectrum of a highly porous dust-free slab exhibits a deep minimum around 25 μm, qualitatively consistent with the TES spectra of the cold spots (see example in Figure 1). As the porosity φ decreases due to densification, the 25-μm band depth BD_{25} decreases, with the brightness temperatures for a nonporous slab approaching the kinetic temperature. Also shown in Figure 2 are spectra computed when, in addition to voids, the slab is assumed to contain 1-μm dust particles with a fractional abundance of 10^{-4} by volume. The dusty spectra have been computed using optical constants for palagonite [34]. In agreement with past investigations [22, 24], the presence of dust reduces the depth of the 25-μm band significantly. The presence of dust is also required to significantly lower the slab albedo. For example, the solar spectral reflectivity of the pure CO_2 slab considered in Figure 2 is close to unity regardless of porosity (except for φ → 0, when the slab albedo approaches the albedo of the underlying surface).

While the spectra shown in Figure 2 are similar to the spectra computed by means of the conventional Mie/delta-Eddington approach [35, 22, 24] (which considers spherical particles *in vacuo*), the chief advantage of the present approach is its connection to the microphysical model of the cap texture and, consequently, its predictive capability. In particular, the present model does not require the notion of meter-sized Mie boulders of solid CO_2 in order to explain the low values of BD_{25} seen in the TES spectra, but instead relates low BD_{25} to low porosity. The strong porosity dependence of the computed BD_{25} suggests that the density evolution obtained from the sintering model can be coupled with the radiative transfer calculations to predict the evolution of BD_{25}. To illustrate this point, in Figure 3 we plot the values of BD_{25} computed from the TES spectra of a narrow zonal sector at the southernmost point of the MGS orbit and compare them with the evolution of BD_{25} predicted by the sintering model. BD_{25} is defined as in [24], with band and continuum channels given in Figure 1. The blue lines represent the evolution computed using the ad-hoc assumption that BD_{25} is inversely proportional to the mean distance $\overline{a}$ between scattering centers and that $\overline{a}$ is, on dimensional grounds, on the order of the ratio (volume)/(internal pore surface area). In the sintering model, this ratio is a weakly nonlinear function of φ, with the result that $BD_{25} \sim \varphi$. Note that the strong $1/r^{3\text{-}4}$ dependence of the densification rate on the grain/void radius [8] provides a stringent constraint on the grain/void size consistent with a seasonal densification timescale. When the volume diffusion coefficient D_v, inferred from NMR measurements [36] is used in the densification equations, the allowable grain/void size is reduced from 10 to about 1 μm as a consequence of a larger activation energy for D_v than assumed previously [8]. This constraint is also of great value in computing the optical properties of the slab. The black and red lines in Figure 3 represent results from the proposed more rigorous approach to the modeling of BD_{25}, in which the evolution of φ computed for r = 1 μm is used to predict the evolution of optical depths and single scattering properties used by the DISORT model. Both dust-free and dusty calculations (as in Figure 2) are presented in Figure 3. For the particular case shown in Figure 3, the computed evolution of BD_{25} is quite different from observations when dust is neglected, but even in this case the proposed model is capable of reproducing the end-member cases of high and low BD_{25} for high and low porosity, respectively. The inclusion of 10^{-4} by volume of dust lowers the computed BD_{25} and improves the agreement with observations (except for the drop in the computed BD_{25} near t = 100 sols).

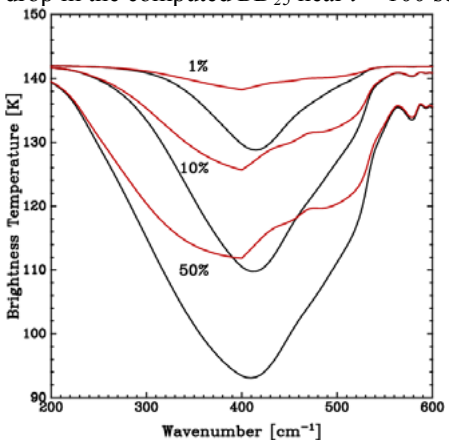

Figure 2: Black curves: spectra of a meter-thick slab of solid CO_2 containing spherical voids with radius 1 μm. The curves are labeled by the value of porosity. These spectra have been computed assuming isothermal conditions at T = 142 K. The red lines show corresponding spectra when in addition to voids the slab contains 1-μm dust particles with an abundance of 10^{-4} by volume.

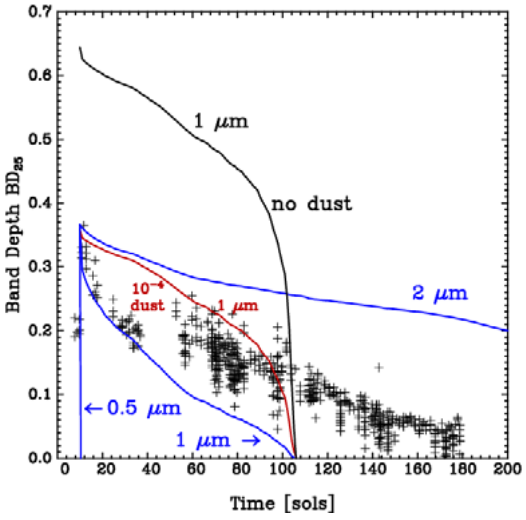

Figure 3: Evolution of BD_{25} in the zonal band 30-40°W in the southern polar ring during the first southern winter of the MGS mapping phase (time is counted from L_s = 107°). Black dots represent individual spectra. The blue curves represent evolutions of BD_{25} computed using the assumption $BD_{25} \sim \varphi$. The black and red curves represent the evolution of BD_{25} computed by coupling the evolution of φ to radiative transfer calculations (the black and red curves correspond to dust-free and dusty slabs, respectively). The curves are labeled by the assumed void size r in the sintering model.

In the future, several important factors not considered in the preliminary analysis presented above should be included, some of which could improve the agreement between the proposed model and observations:

- In the above calculations, the slab thickness has been assumed constant at L = 1 m. In reality, the slab thickness will change in the course of a season as a result of condensation, densification, and sublimation. In future work, a more realistic approach could be adopted, in which L is constrained by the MOLA data (such as Fig. 2 in [23]). The use of a realistic evolution of L might necessitate a consideration of a non-homogeneous density distribution with depth (with younger frosts being fluffier than older deposits). Deposition of fresh frost is likely to reduce the sharp drop in the computed BD_{25} seen in Figure 3.
- As mentioned above, the void size r strongly affects densification rate. The value of r consistent with observed evolution of BD_{25} is dependent on the adopted value for the volume diffusion coefficient D_v and the sensitivity of the estimated r to the measurement uncertainties in D_v [36], as well as possible changes in r in the course of the densification process need to be evaluated.
- The sealing-off of the pore space will lead to the formation of a thermal gradient. This will affect radiative transfer in the slab, both directly and by increasing the void size consistent with seasonal densification (with the concomitant effect on the optical properties of the slab).

Implications: The new model presented herein will aid in the analysis of data from instruments employing both remote (visible, infrared, radar) and *in situ* (e.g., drilling) technology. For example, the model of CO_2 surface emissivity could constrain retrievals from nadir-looking IR-sounders over the martian polar regions, in a somewhat analogous manner as models of ocean IR emissivity provide the *a prori* information for retrievals from terrestrial infrared sounders. Moreover, since the radiative properties of the CO_2 deposits exert a strong control on the martian atmosphere, the new model is relevant to meteorological and climate studies of Mars.

Acknowledgements: Dr. Ping Yang of Texas A&M University is thanked for making available the Mie code. This work has been funded in part by the Mars Data Analysis Program.

References: [1] Moroz V. I. (1964) *Sov. Astron. 8,* 273. [2] Kieffer H. (1970) *JGR, 75,* 510. [3] Larson H. P. and U. Fink (1972) *ApJ. Lett., 171,* 91. [4] Calvin W. M. (1990) *JGR, 95,* 14,743. [5] James P. B. et al. (1979) *JGR, 84,* 2889. [6] Paige D. A. and A. P. Ingersoll (1985) *Science, 228,* 1160. [7] Lindner B. L. (1992) *GRL, 19,* 1675. [8] Eluszkiewicz J. (1993) *Icarus, 103,* 43. [9] Eluszkiewicz J. (1991) *JGR, 96,* 19,217. [10] Cruikshank D. et al. (1984) *Icarus, 58,* 293. [11] Kirk R. L. et al. (1990) *Science, 250,* 424. [12] Moore J. M. and J. R. Spencer (1990) *GRL, 17,* 1757. [13] Helfenstein P. J. et al. (1992) *Science, 255,* 824. [14] Lee P. et al. (1992) *Icarus, 99,* 82. [15] Soderblom L. A. et al. (1990) *Science, 250,* 410. [16] Kieffer, H. H. (2000) *Science, 289,* 1853. [17] Calvin W. M. and T. Z. Martin (1994) *JGR, 99,* 21,143. [18] Butler B. J. (1994) Ph.D. thesis, Caltech. [19] Paige D. A. et al. (1995) *BAAS, 27,* 1098. [20] Forget F. and J. B. Pollack (1995) *JGR, 101,* 16,865. [21] Forget F. et al. (1998) *Icarus, 131,* 302. [22] Hansen G. B. (1999) *JGR, 104,* 16,471. [23] Smith D. E. et al. (2001) *Science, 294,* 2141. [24] Kieffer H. et al. (2000) *JGR, 105,* 9653. [25] Titus T. N. et al. (2001) *JGR, 106,* 23,181. [26] Adissin A. et al. (1977) *Trans. J. Br. Ceram. Soc., 76,* 17. [27] Markham J. R. et al. (1992) *J. Heat Transfer, 114,* 458. [28] Kieffer H. (1968) Ph.D. thesis, Caltech. [29] Hansen G. B. (1997) *JGR, 102,* 21,569. [30] Swinkels F. B. and M. F. Ashby (1981) *Acta Metall., 29,* 259. [31] Wood S. E. (1998) Ph. D. thesis, UCLA. [32] Yang P. et al. (2002) *Appl. Opt., 41,* 2740. [33] Stamnes K. et al. (1988) *Appl. Optics, 27,* 2502. [34] Roush T. et al. (1991) *Icarus, 94,* 191. [35] Warren S. et al. (1990) *JGR, 95,* 14,717. [36] Liu S.-B. et al. (1985) *J. Chem. Phys., 81,* 6064.